6. R. E. Burke, *Movement Disorders* **1**, 135 (1986); S. B. Freedman, M. S. Beer, E. A. Harley, *Eur. J. Pharmacol.* **156**, 133 (1988).
7. B. E. Marshall and D. E. Longnecker, in *Goodman and Gilman's The Pharmacological Basis of Therapeutics*, A. G. Gilman, T. W. Rall, A. S. Nies, P. Taylor, Eds. (Pergamon, New York, 1990), p. 307.
8. D. L. Reich and G. Silvay, *Can. J. Anaesth.* **36**, 186 (1989); E. N. Ayim and F. X. Makatia, *East Afr. Med. J.* **53**, 377 (1976); K. Korttila and J. Levanen, *Acta Anaesthesiol. Scand.* **22**, 640 (1978); D. L. Coppel, J. G. Bovill, J. W. Dundee, *Anaesthesia* **28**, 293 (1973).
9. Rats (n = 6) were treated with a standard dose of MK-801 (0.4 mg/kg sc), then anesthetized with halothane, and maintained under halothane anesthesia for 4 hours. When killed at 4 hours, all rats in both groups had an abundant display of vacuolated neurons in the cingulate and retrosplenial cortices.
10. J. W. Sharp, S. M. Sagar, F. R. Sharp, *Soc. Neurosci. Abstr.* **16**, 1122 (1990).
11. M. A. Sesma, M. T. Price, J. W. Olney, *ibid.*, in press. We localized HSP immunocytochemically using a primary antibody directed against HSP72 (Amersham RPN 1197) and a modified Vector Elite avidin-biotin-peroxidase (ABC) method recommended by F. R. Sharp (*9*). An antisera-free incubation served as an internal control for each case.
12. R. L. Macdonald and J. L. Barker, *Science* **200**, 775 (1978); E. S. Levitan, L. A. Blair, V. E. Dionne, E. A. Barnard, *Neuron* **1**, 773 (1980); N. Akaike, T. Maruyama, N. Tokutomi, *J. Physiol. (London)* **394**, 85 (1987); C. F. Zorumski and K. E. Isenberg, *Am. J. Psychiatry* **148**, 162 (1991).
13. R. E. Study and J. L. Barker, *Proc. Natl. Acad. Sci. U.S.A.* **78**, 7180 (1981).
14. J. A. O. Magbagbeola and N. A. Thomas, *Can. Anaesth. Soc. J.* **21**, 321 (1974).
15. The proposal that the pathomorphological and psychotomimetic side effects of NMDA antagonists may be causally linked rests on the reasonable assumption that reversible injury confined to cingulate-retrosplenial neurons might produce a temporary derangement in psychological functions mediated by any or all components of an extensive neural network with which these neurons communicate.
16. Behavioral side effects of competitive and noncompetitive NMDA antagonists are similar and consist of ataxia and hyperactivity at low to moderate doses, with a progressive increase in muscle tone at higher doses that causes the animals to lie on their sides with partially flexed limbs held in a rigid posture. Anticholinergic drugs were well tolerated; in fact, they tended to relieve these symptoms, especially the muscular rigidity. Treatment with an NMDA antagonist plus a barbiturate was also well tolerated. Consistent with the barbiturate effect alone, the animals appeared heavily sedated, but there was no apparent potentiation by the barbiturate of the NMDA antagonist's effects or vice versa, and respiratory function was not compromised.
17. Certain barbiturates, especially thiamylal, effectively block both NMDA and non-NMDA subtypes of glutamate receptor and can prevent ischemic neuronal degeneration [J. Olney *et al.*, *Neurosci. Lett.* **68**, 29 (1986); J. Olney, in *Excitatory Amino Acids in Health and Disease*, D. Lodge, Ed. (Wiley, London, 1988), pp. 337–352]. Thus, barbiturates are neuroprotective in a dual sense. They protect against ischemic neuronal degeneration in many brain regions by blocking glutamate (including NMDA) receptors, while preventing NMDA antagonist neurotoxicity in the cingulate cortex by exerting GABAmimetic activity that is stronger than their NMDA antagonist activity.
18. G. Paxinos and C. Watson, *The Rat Brain in Stereotaxic Coordinates* (Academic Press, New York, 1982).

19. We thank F. R. Sharp for advice on immunohistochemical methods. Supported in part by a grant from the Huntington's Disease Foundation, PHS grants DA 53568 and AG 05681, National Institute of Mental Health Research Scientist Award MH 38894 (J.W.O.), a Weldon Spring Fund grant, and a Research Leave Award from the University of Missouri–St. Louis (M.A.S.).

8 August 1991; accepted 10 October 1991

Functional Contribution of Neuronal AChR Subunits Revealed by Antisense Oligonucleotides

MARK LISTERUD,* ARJEN B. BRUSSAARD,* PÍRESKA DEVAY,* DAVID R. COLMAN, LORNA W. ROLE†

Although multiple related genes encoding nicotinic acetylcholine receptor (AChR) subunits have been identified, how each of these subunits contributes to AChRs in neurons is not known. Sympathetic neurons express four classes of AChR channels and six AChR subunit genes (α3, α4, α5, α7, β2, and β4). The contribution of individual subunits to AChR channel subtypes in these neurons was examined by selective deletion with antisense oligonucleotides. An α3 antisense oligonucleotide decreased the number and altered the properties of the normally expressed ACh-activated channels. The remaining AChR channels have distinct biophysical and pharmacological properties that indicate an important functional contribution of the α7 subunit.

LIGAND-GATED ION CHANNELS ARE multimeric protein complexes with component subunits encoded by homologous genes (*1*). The neuronal nicotinic AChRs that mediate neurotransmission at many central and peripheral synapses comprise two subunit types (α and β) encoded by at least 11 related genes (*2*). Expression of particular combinations of the subunit RNAs in oocytes yields biophysically and pharmacologically distinct channels (*3*), reminiscent of the multiple AChR channel types detected in embryonic sympathetic neurons (*4*). However, neither the identity nor the functional contribution of the individual α and β subunits in native AChR channel subtypes is known.

To determine which AChR subunit genes are expressed by sympathetic neurons, we used the polymerase chain reaction (PCR) (*5*). Primers to the nonconserved regions of the α and β subunit genes were chosen to amplify specific cDNA target sequences (Fig. 1A). Appropriate-sized products were generated in the α3, α4, α5, α7, and β reactions, but not in the α2 reaction (Fig. 1B) (*6*). Restriction enzyme digestion of the amplified products confirmed their identity. RNA blots of polyadenylated [poly(A)$^+$] RNA from sympathetic ganglia under stringent hybridization and washing conditions revealed hybridization to α3, α4, α5, α7, β2 (n-α), and β4 (n-α3) probes but not to the α2 probe (Fig. 1C) (*7*). AChR gene expression ranged from undetectable (α2) and low (α4, α5, β2) to relatively high (α3, α7, β4).

Because sympathetic neurons express multiple types of α and β subunit genes, the AChR channel subtypes observed (*4*) might result from different subunit combinations. To determine the role of individual AChR subunits in sympathetic neurons, we examined changes in the properties of AChR channels after functional deletion of a particular subunit with antisense oligonucleotides.

The contribution of preexistent surface AChRs was removed by treatment with bromoacetylcholine (BAC), which covalently binds to and inactivates AChRs (*8*). BAC-treated neurons regain ACh sensitivity through synthesis of new AChRs (*9*). ACh sensitivity was <15% of control at 3 hours and completely restored within 48 hours of BAC treatment (*9*). Sympathetic neurons were incubated with oligonucleotide immediately after BAC treatment, and the ACh-activated single channel currents were measured after 48 hours (*10*). Analysis of the number of channel openings and the averaged single channel current from all patches in α3 antisense–oligonucleotide treated neurons indicates a >90% decrease from the control levels of AChR channel activity typically evoked by 2.5 μM ACh (Fig. 2) (*11*). Although the number of AChR channel openings under these conditions was too low for slope conductance determinations, the residual activity included openings at amplitudes consistent with the characterized AChR subtypes (designated S, M, L, and XL) (*4*). An α4 antisense (Fig. 2) as well as several control oligonucleotides (*10*) did not affect AChR channel opening frequency, mean current, conductance, or desensitization kinetics. In view of these results and the lack of effect on other ligand or voltage-gated channels (*10*), it seems likely that α3 antisense reduces AChR channel activity by a specific functional deletion of the α3 subunit.

The observed decrease in AChR channel activity gated by 2.5 μM ACh is apparently due to both an increase in the ACh concentration required for channel activation and a decrease in the number of functional AChRs (Figs. 3 and 4). In patches from control

Departments of Anatomy and Cell Biology, Pathology, and the Center for Neurobiology and Behavior, Columbia College of Physicians and Surgeons, New York, NY 10032.

*The first three authors contributed equally.
†To whom correspondence should be addressed.

neurons, higher concentrations of ACh (25 μM) gate all four AChR channel classes (*4*), but these channels desensitize rapidly (Fig. 3, A through C). In contrast, in patches from neurons treated with α3 antisense, 25 μM ACh elicited persistent AChR single channel activity (Fig. 3F). Analysis of AChR openings in α3 antisense–treated neurons revealed two conductance classes similar to those in control neurons and, in addition, a conductance class of ~115 pS (Fig. 3 D, E). All of the channels in α3 antisense–treated neurons differed from control in requiring a higher concentration of ACh for their activation and in their slower desensitization in the continued presence of ACh.

Examination of macroscopic currents evoked by maximal concentrations of ACh reveals a significant decrease in the total number of functional AChRs in α3 antisense–treated neurons compared with control neurons (~60% decrease in the average peak current; Fig. 4, A and C). This analysis underestimates the decrease in AChRs, however, because of significant slowing of AChR desensitization after α3 antisense treatment (*12*). High concentrations of ACh normally evoke currents that decay with a biphasic time course (Fig. 4A). In contrast, in neurons treated with α3 antisense, macroscopic currents evoked by the same concentration of ACh desensitized at a slower rate reflected in a significant increase in both the fast and slow time constants of desensitization (Fig. 4, A and D).

We next sought to identify which α subunit might contribute to the new, slowly desensitizing currents evoked by ACh in neurons where α3 had been functionally deleted. Because the α5 subunit gene fails to yield functional AChR channels when coexpressed in oocytes with either β2 or β4 genes (*13*), α7 seemed the best candidate for the ligand-binding subunit in the novel AChRs expressed by neurons treated with α3 antisense. The role of α7 in the AChRs was tested two ways. The α7 subunit, unlike α3, is blocked by α-bungarotoxin (α-BGT) (*14*). If α7 is an important component of the AChRs, then the slowly desensitizing current in neurons treated with α3 antisense should be eliminated by α-BGT. Similarly, oligonucleotide-mediated deletion of α7 should have quantitatively the same effect as α-BGT treatment, if α7 participates in these AChRs. Both these predictions are supported by the experiments in Fig. 4.

ACh-activated currents in control neurons were unaffected by α-BGT. However, in α3 antisense–treated neurons the toxin decreased the peak of macroscopic currents by 60 to 70% (Fig. 4, A and C). The residual, α-BGT insensitive current was blocked by neuronal bungarotoxin (nBGT) and desensitized rapidly, which are features characteristic of control AChR currents (Fig. 4D) (*15*). Treatment with an α7 antisense decreased control ACh-evoked currents by <25%. However, like α-BGT, the α7 antisense decreased the ACh-evoked currents by 60 to 70% in α3 antisense–treated neurons (Fig. 4, B and C). The residual current (*15*) also resembled control ACh-evoked currents: it desensitized with kinetics equivalent to control, exhibited insensitivity to α-BGT (Fig. 4D), and was blocked by nBGT. Thus, the slowly desensitizing AChRs expressed in α3 antisense–treated neurons are blocked by α-BGT and dependent on the expression of α7. This indicates that α7 may be the principal ligand-binding subunit of the AChR channels expressed after functional deletion of α3.

Treatment of embryonic chick sympathetic neurons with antisense oligonucleotides against α3, α4, or α7 subunit sequences suggests specific functional contributions of these subunits to neuronal AChRs. The α3 subunit appears to play an important role in all four AChR channel classes normally expressed by these neurons. The functional deletion of the α3 subunit decreases the number of openings of all channel subtypes, alters the concentration of ACh sufficient to

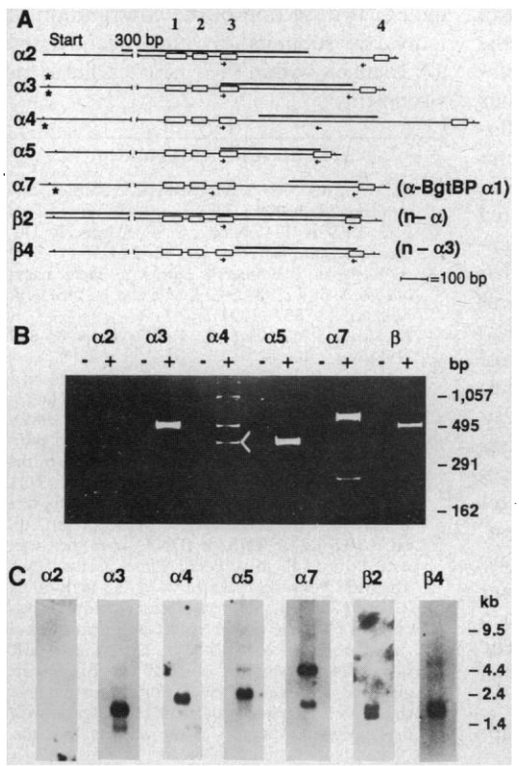

Fig. 1. AChR subunit gene expression in sympathetic neurons. (**A**) Diagram of neuronal AChR cDNA sequences. Proposed transmembrane-spanning domains are indicated by boxes; arrows indicate the regions used for PCR primers; bold lines indicate the fragments used to generate probes for Northern (RNA) blots, and asterisks near the start sites indicate the region used for functional block oligonucleotides (*6, 10*). (**B**) PCR assay of embryonic day 10 sympathetic ganglia RNA with (+) or without (−) previous cDNA synthesis (*6*). (**C**) Northern (RNA) analysis of ED 10 sympathetic ganglia poly A^+ RNA (7). Approximate sizes: α3: 2.0 kb, α4: 2.4 kb, α5: 2.9 kb, α7: 2.3 and 5.0 kb, β2: 1.8 and 1.5 kb, β4: 1.9 kb.

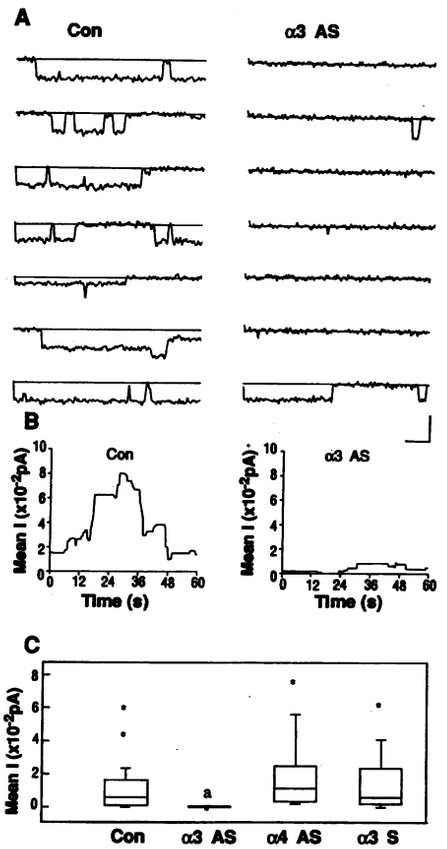

Fig. 2. AChR channel activity is decreased in α3 antisense–treated neurons (*10, 11*). (**A**) Nonconsecutive traces from cell-attached patches on control and α3 antisense–treated neurons (2.5 μM ACh, V_h: −50 mV relative to rest, 5 pA × 5 ms). (**B**) Mean current versus time for patches in (A). Average mean current values over 3 min were 0.0323 (Con) and 0.0031 (α3 AS). (**C**) Box plot representation of mean current determinations. Control: n = 30, α3 antisense: n = 27, α4 antisense: n = 9, α3 sense: n = 18. The α3 antisense group (a) is significantly different ($P \leq 0.001$) from other groups. Examination of channel opening frequency yielded identical results.

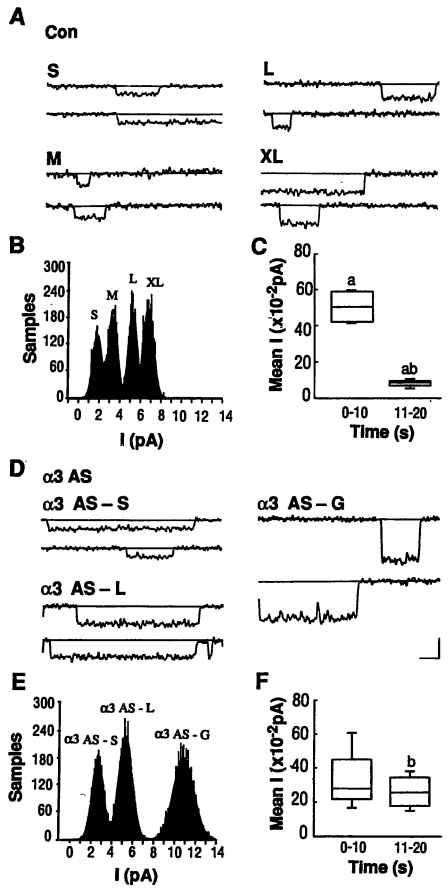

Fig. 3. α3 antisense-treated neurons express novel AChR channels (*10, 11*). High concentrations of ACh activate three AChR subtypes in α3 antisense–treated neurons. (**A**) Nonconsecutive records of channels activated by 25 μM ACh in control neurons. S, M, L, XL subtypes with $\gamma \pm$ SD of 17 ± 5.1, 31 ± 5.9, 49 ± 4.7, and 65 ± 4.6 were detected. (**B**) Amplitude histogram of channels (Con) with summed Gaussian fit superimposed. (**D**) Nonconsecutive records of channels gated by 25 μM ACh from α3 antisense–treated neurons. Three AChR subtypes designated α3 AS-S (small), α3 AS-L (large), and α3 AS-G (giant) with $\gamma \pm$ SD of 24 ± 9.5, 53 ± 6.0, and 114 ± 13.0, respectively, are seen. (**E**) Amplitude histogram of channels (α3 AS) with summed Gaussian fit superimposed. All openings required ACh and were blocked by hexamethonium (500 μM). (Cell-attached patches; V_h: −50 mV relative to rest for (A) and (B); 5 pA × 5 ms). (**C**) and (**F**): Desensitization of AChR openings analyzed by comparison of mean single-channel current over two consecutive 10-s periods of ACh application to outside-out patches from control and α3 antisense–treated neurons (V_h: −100 mV; ACh: 25 μM). Boxplots of data from all patches indicate persistent ACh-gated single channel activity in α3 antisense–treated neurons compared with control (a and b pair, $P \leq 0.001$).

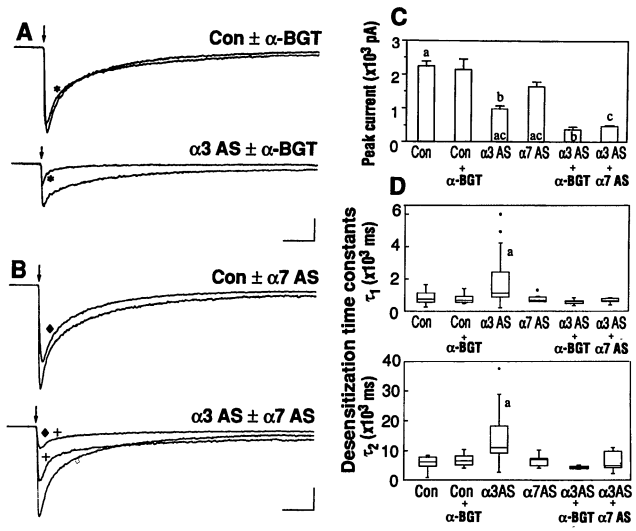

Fig. 4. Both α-bungarotoxin and α7 antisense alter ACh-evoked currents in α3 antisense–treated neurons (*10, 11*). (**A**) Macroscopic currents from control and α3 antisense–treated neurons before and after (*) α-BGT application (ACh: 500 μM; α-BGT: 500 nM, 10 min) and (**B**) (top) Macroscopic currents from control and α7 antisense–treated neuron (♦), and (bottom) macroscopic currents from control versus α3 antisense–treated neurons (+) versus neuron treated with both α3 antisense and α7 antisense (+ and ♦; V_{hold}: −50 mV; 500 pA × 1 s). nBGT completely blocked ACh-evoked currents in control and in α3 plus α7 antisense-treated neurons. (**C**) Summary of peak macroscopic current data (mean ± SEM) (**D**) Summary of desensitization time course data. Fast (τ_1) and slow (τ_2) time constants of the biexponential decay of the macroscopic currents are displayed with boxplots. Control: $n = 27$; +α-BGT: $n = 10$; α3 antisense-treated: $n = 26$; α7 antisense-treated: $n = 7$, α3 antisense-treated +α-BGT: $n = 15$; α3 antisense + α7 antisense-treated: $n = 8$. In (C) the comparisons (a) were significantly different ($p \leq 0.001$) for control versus α3 AS, at $P \leq 0.023$ for control versus α7 AS; (b) indicates $p \leq 0.004$ for α3 AS versus α3AS + α-BGT; (c) indicates $P \leq 0.041$ for α3 AS versus α3 AS + α7 AS; $p \leq 0.001$ for α7 AS versus α3AS + α7 AS. In (D), (a) indicates differences at $P \leq 0.004$ to 0.001 for α3 AS versus all other groups. The relative contribution of the fast and the slow time constant did not differ among groups. α-BGT did not affect either peak current or decay in α4 antisense-treated neurons.

gate channel activity, alters AChR desensitization, and results in the expression of a new, larger conductance AChR channel. Biochemical and molecular studies have also indicated that the α3 subunit is a component of peripheral neuronal AChRs (*16*).

After functional deletion of α3, a new class of channels emerges that appears to be dominated by the α7 subunit. Because treatment with α7 antisense alone significantly decreased the control ACh-evoked current, α7 is likely a component subunit of the AChR channels normally expressed in sympathetic neurons. However, α-BGT, which blocks α7 subunit homooligomers in the oocyte (*14*), does not decrease the control ACh-evoked currents (Fig. 4). Thus, the AChRs in neurons that include the α7 subunit or subunits must include other subunits that are α-BGT–resistant (α3) or that influence the α-BGT sensitivity of the α7 subunit (*17*). Furthermore, because macroscopic ACh-evoked currents, which are mediated by α7 homooligomers in the oocyte, desensitize rapidly (*14*), our findings suggest that other factors [for example, different subunit combinations or posttranslational modification (*18*)] are important determinants of AChR desensitization kinetics in neurons. Homooligomers of α7 mediate a large ACh-evoked macroscopic current in the oocyte (*14*) consistent with our finding an unusually large conductance channel. Although α4 is expressed in sympathetic neurons, treatment of cells with an α4 antisense had no effect on AChR-activated currents. If the α4 antisense functionally deletes α4, then expression of a given AChR subunit gene may not indicate participation in functional AChR channels.

These studies also provide a general approach for the dissection of receptor function in primary neurons that complements studies in heterologous cell expression systems. The use of antisense oligonucleotides to unravel the functional contribution of individual subunits is applicable to the analysis of AChRs in other regions of the nervous system (*19*) and should permit the molecular dissection of the contribution of individual subunits to other ligand-gated ion channels within their native cellular environment.

REFERENCES AND NOTES

1. R. M. Stroud, M. P. McCarthy, M. Shuster, *Biochemistry* **29**, 11009 (1990).
2. E. S. Deneris, J. Connolly, S. W. Rogers, R. Duvoisin, *Trends Pharmacol. Sci.* **12**, 34 (1991).
3. R. L. Papke, J. Boulter, J. Patrick, S. Heinemann, *Neuron* **3**, 589 (1989); C. Luetje and J. Patrick, *J. Neurosci.* **11**, 837 (1991).
4. B. Moss, S. Schuetze, L. Role, *Neuron* **3**, 597 (1989).
5. J. Sambrook, E. F. Fritsch, T. Maniatis, *Molecular Cloning, A Laboratory Manual* (Cold Spring Harbor Laboratory, Cold Spring Harbor, NY, ed. 2, 1989).
6. Polymerase chain reaction (PCR) assay: RNA purified from ED10 or ED17 sympathetic ganglia by the guanidium-CsCl centrifugation method (*5*). RQ1 DNase-treated total RNA served as template for first strand synthesis (AMV reverse transcriptase). Aliquots (0.5 μg of RNA or cDNA) were then submitted to PCR in a Perkin-Elmer Cetus DNA Thermal Cycler: 35 cycles of 94°C, 0.5 min; 40°C, 0.5 min; 75°C, 0.75 min. Reverse transcriptase was omitted from the cDNA synthesis reaction before amplification in controls (−). The same AChR subunits were expressed in ED10 and ED17 ganglia. The α2 target can be amplified from genomic chick DNA (digested with Eco RI and Bgl II) with the appropriate primers. Sense primers: α3, α5:

CTCCTCTTCAC(C/T)ATGATATTTGT; α2, α4 CTCTTCACCATGAT(A/C)TTTG; α7: ATGCCAGCAACATCTGATTCT and β TGGT(A/G)CTGGTGACCTTCTC. Antisense primers: (reverse complement of sequences specified by number) α2: 1367 to 1386; α3: 1305 to 1325; α4: 1201 to 1221; α5: 1164 to 1184; α7: TACTACAGAGGCTGCAAACTT and β: ACCATGGC(A/C)AC(A/G)TACTT.

7. We ran 2.5 μg of poly(A)$^+$ RNA from ED10 sympathetic ganglia per lane on a formaldehyde (1%) agarose gel and blotted it onto Nytran (Schleicher and Schuell) for hybridization, according to the manufacturer's instructions. Probes generated by random primer synthesis (Promega) to a specific activity of ≥5 × 10^8 cpm/μg. Following the lack of hybridization to α2 probe, the lane was rehybridized to other probes to confirm RNA retention on the blot.
8. I. Silman and A. Karlin, *Science* **164**, 1420 (1969).
9. R. Gardette *et al.*, *Dev. Biol.* **147**, 83 (1991).
10. Methods: E10 and 11 chick lumbar sympathetic ganglion neurons were prepared as described (*4*) and plated in dishes with a 13-mm sunken well of ~150 μl. BAC bromide treatment was modified from P. Leprince [*Biochemistry* **22**, 5551 (1983) (*9*)]. Oligonucleotide treatment: Functional block oligonucleotides: α3 sense and antisense −77 to −63; α3 mismatch antisense CGACCGTAAAACAAC; α4 antisense −69 to −55; α7 antisense GCATCAGCGCCCGGA. Oligos made on Applied Biosystems Automated DNA Synthesizer (380B) and purified by polyacrylamide gel electrophoresis and reversed-phase chromatography (*5*). No known chick AChR sequences are complementary to these 15-mers (optimal complementarity with other AChR sequences ≤72%). Oligonucleotides in growth media (*4*) were added to neurons within culture wells and maintained in a humidified chamber (48 hours). Additional antisense controls: neither inclusion of α3 antisense in the recording pipette nor treatment of neurons with oligonucleotides similar to α3 in size, charge, or sequence (three base mismatch) had any effect on AChR function. K$^+$-channel activity and GABA-evoked currents were unaltered in antisense-treated neurons.
11. Single channel and macroscopic current analysis. Data acquisition and analysis used BASIC 23–based software developed by S. Schuetze (*4*) or S. Siegelbaum. Slope conductance determined from recordings at −30, −50, and −70 mV relative to rest. We obtained mean single channel current activity in individual patches by integrating t(open)/t(total) for the first 3 min (cell-attached patch) or for 10 s after agonist application (outside-out). The decay time course of macroscopic currents was fit by the sum of two exponential functions (fast and slow time constants τ_1 and τ_2). Presentation and statistics. Mean single channel current and macroscopic current decay time constant data were not normally distributed and therefore are presented in box plots. The central box shows the middle 50% of the data (25th through 75th percentiles); the horizontal line indicates the median, and the whiskers indicate the range of data values (10th through 90th percentiles). Outliers, if present, are plotted as asterisks. Mean current and decay constants of control groups were normalized to permit statistical comparison between corresponding experimental groups. The values obtained were normally distributed following log transformation [Kolmogorov-Smirnov test; G. W. Snedecor and W. G. Cochran, *Statistical Methods* (Iowa State Univ. Press, Ames, IA, ed. 6, 1967), p. 329; NPAR and MGLH modules of Systat™]. Subsequent analysis of variance (ANOVA) was followed by a test for multiple comparisons between pairs of group means based on unequal sample sizes.
12. AChR number in α3 antisense–treated neurons: ACh dose response data indicate that 500 μM evokes a maximal response in both control and α3 antisense–treated neurons. Mathematical subtraction of the contribution of slower desensitization indicates that α3 antisense decreased the number of activatable AChRs by >65% (rather than 58%). This correction is still an underestimate because it assumes comparable single-channel conductances in α3 antisense–treated and control neurons whereas larger conductance channels predominate in α3 antisense–treated neurons. (L versus α3 AS-L: 66% versus 89% of patches; XL versus α3 AS-Giant: 37% versus 52% of patches).
13. S. Couturier *et al.*, *J. Biol. Chem.* **265**, 17560 (1990).
14. S. Couturier *et al.*, *Neuron* **5**, 847 (1990).
15. The residual current in neurons treated with α3 antisense plus α7 antisense or α-BGT resembles control in desensitization kinetics and in its complete block by nBGT [R. Loring and R. Zigmond, *Trends Neurosci.* **11**, 73 (1988)]. This current may be composed of native receptors assembled from the internal pool or due to delayed or incomplete antisense-mediated deletion.
16. R. T. Boyd *et al.*, *Neuron* **1**, 495 (1988); R. Schoepfer *et al.*, *FEBS Lett.* **257**, 393 (1989).
17. P. Blount and J. P. Merlie, *Neuron* **3**, 349 (1989).
18. R. L. Huganir and P. Greengard, *ibid.* **5**, 555 (1990).
19. A. Brussaard, J. Doyle, L. Role, in preparation.
20. We thank R. Axel, T. Jessell, A. Karlin, and S. Siegelbaum (Columbia College of Physicians and Surgeons) for discussions, reagents, and extensive comments on the manuscript; M. Ballivet and collaborators from the University of Geneva for sharing clones and sequence information before publication; and D. King, A. Roy, A. Dolorico, A. Witty, and E. Hubel for technical assistance. Supported by awards from NSF, North Atlantic Treaty Organization, Muscular Dystrophy Association, NIH (NS27680, NS 29071), and the Council for Tobacco Research.

12 June 1991; accepted 10 October 1991

Refined Structure of Charybdotoxin: Common Motifs in Scorpion Toxins and Insect Defensins

FRANCOIS BONTEMS, CHRISTIAN ROUMESTAND, BERNARD GILQUIN, ANDRÉ MÉNEZ, FLAVIO TOMA

Conflicting three-dimensional structures of charybdotoxin (Chtx), a blocker of K$^+$ channels, have been previously reported. A high-resolution model depicting the tertiary structure of Chtx has been obtained by DIANA and X-PLOR calculations from new proton nuclear magnetic resonance (NMR) data. The protein possesses a small triple-stranded antiparallel β sheet linked to a short helix by two disulfides and to an extended fragment by one disulfide, respectively. This motif also exists in all known structures of scorpion toxins, irrespective of their size, sequence, and function. Strikingly, antibacterial insect defensins also adopt this folding pattern.

CHARYBDOTOXIN (CHTX) IS A TOXIN acting on K$^+$ channels isolated from venom of a scorpion (*Leiurus quinquestriatus hebraeus*) (*1*). It is a small protein, containing 37 amino acids and three disulfide bridges (*2*). Elucidation of its three-dimensional (3-D) structure is important for understanding the molecular basis of its activity and for designing drugs acting on K$^+$ channels. The structure of Chtx has been reported in two recent NMR studies (*3, 4*) that led to different 3-D models of the toxin. One of these has now been retracted (*5*). Also, a recent communication has reported the preliminary NMR structure of synthetic Chtx (*6*) that is similar to that obtained in our work. We have collected additional NMR data from which further Chtx structures have been computed. The new refined structures confirm our initial model (*4*) and show that Chtx possesses a motif that is conserved in functionally unrelated proteins of arthropods.

We have reported elsewhere the sequence-specific assignments of the ^{1}H NMR spectra, the identification of the secondary structure elements, and the tertiary structure computations (*4*). The new data, recorded at temperatures from 15° to 45°C, include NOEs (eight mixing times from 50 to 300 ms), HN-Hα and Hα-Hβ vicinal coupling constants, and amide ^{1}H-^{2}H exchange rates at 15°C. Iteration of back calculations and analysis of NOESY experiments led to the assignment of 144 interresidue NOE connectivities that correspond to 72 sequential and 72 nonsequential effects (Fig. 1). Intensities of backbone-backbone NOEs were determined either from NOE buildup rates or from cross-peak volumes in spectra recorded with a 150-ms mixing time. The corresponding distance constraints were obtained calibrating the backbone-backbone NOE intensities with known distances in regular secondary structures (2.2 Å for $d_{\alpha N}$ in a β sheet and 2.8 Å for d_{NN} in an α helix). Measurement of the exchange rates of amide protons allowed the identification of 11 hydrogen bonds, leading to the introduction of 22 additional constraints. In addition, 12 χ1-angle values, including those of the six half-cystines, were deduced from the measurement of $^3J_{H\alpha\text{-}H\beta}$ and the identification of intraresidue HαHβ NOEs, whereas 30 φ-angle values were deduced from the values of $^3J_{HN\text{-}H\alpha}$ coupling constants.

The 3D-structures of Chtx were derived from these data with a procedure that combined minimization in the dihedral angle

Département d'Ingénierie et d'Etudes des Protéines, CEN Saclay, 91191 Gif sur Yvette, France.